Video Article

Merging Ion Concentration Polarization between Juxtaposed Ion Exchange Membranes to Block the Propagation of the Polarization Zone

Minyoung Kim[1,2], Hyunjoon Rhee[1,3], Ji Yoon Kang[1], Tae Song Kim[1], Rhokyun Kwak[1]

[1]Center for BioMicrosystems, Korea Institute of Science and Technology

[2]Department of Mechanical Engineering, Seoul National University

[3]Department of Industrial Engineering, University of Illinois Urbana-Champaign

Correspondence to: Rhokyun Kwak at rhokyun@kist.re.kr

URL: https://www.jove.com/video/55313
DOI: doi:10.3791/55313

Keywords: Bioengineering, Issue 120, ion concentration polarization, preconcentration, ion exchange membrane, overlimiting current, electro-osmotic flow, electro-osmotic instability

Date Published: 2/23/2017

Citation: Kim, M., Rhee, H., Kang, J.Y., Kim, T.S., Kwak, R. Merging Ion Concentration Polarization between Juxtaposed Ion Exchange Membranes to Block the Propagation of the Polarization Zone. *J. Vis. Exp.* (120), e55313, doi:10.3791/55313 (2017).

Abstract

The ion concentration polarization (ICP) phenomenon is one of the most prevailing methods to preconcentrate low-abundance biological samples. The ICP induces a noninvasive region for charged biomolecules (*i.e.,* the ion depletion zone), and targets can be preconcentrated on this region boundary. Despite the high preconcentration performances with ICP, it is difficult to find the operating conditions of non-propagating ion depletion zones. To overcome this narrow operating window, we recently developed a new platform for spatiotemporally fixed preconcentration. Unlike preceding methods that only use ion depletion, this platform also uses the opposite polarity of the ICP (*i.e.,* ion enrichment) to stop the propagation of the ion depletion zone. By confronting the enrichment zone with the depletion zone, the two zones merge together and stop. In this paper, we describe a detailed experimental protocol to build this spatiotemporally defined ICP platform and characterize the preconcentration dynamics of the new platform by comparing them with those of the conventional device. Qualitative ion concentration profiles and current-time responses successfully capture the different dynamics between the merged ICP and the stand-alone ICP. In contrast to the conventional one that can fix the preconcentration location at only ~5 V, the new platform can produce a target-condensed plug at a specific location in the broad ranges of operating conditions: voltage (0.5-100 V), ionic strength (1-100 mM), and pH (3.7-10.3).

Video Link

The video component of this article can be found at https://www.jove.com/video/55313/

Introduction

Ion concentration polarization (ICP) refers to a phenomenon that occurs during ion enrichment and ion depletion on a permselective membrane, resulting in an additional potential drop with ion concentration gradients[1,2]. This concentration gradient is linear, and it becomes steeper as a higher voltage is applied (Ohmic regime) until the ion concentration on the membrane approaches zero (limiting regime). At this diffusion-limited condition, the gradient (and corresponding ion flux) has been known to be maximized/saturated[1]. Beyond this conventional understanding, when the voltage (or current) is increased further, an overlimiting current is observed, with flat depletion zones and very sharp concentration gradients at the zone boundary[1,3]. The flat zone has a very low ion concentration, but surface conduction, electro-osmotic flow (EOF), and/or electro-osmotic instability promote ion flux and induce an overlimiting current[3,4,5]. Interestingly, the flat depletion zone serves as an electrostatic barrier, which filters out[6,7,8,9] and/or preconcentrates targets[10,11]. Since there is an insufficient amount of ions to screen the surface charges of charged particles (for satisfying electroneutrality), the particles cannot pass through this depletion zone and therefore line up at its boundary. This nonlinear ICP effect is a generic phenomenon in various types of membranes[10,11,12,13,14] and geometries[6,15,16,17,18,19,20,21]; this is why researchers have been able to develop various types of filtration[6,7,8,9] and preconcentration[10,11] devices using the nonlinear ICP.

Even with such high flexibility and robustness, it is still a practical challenge to clarify the operating conditions for the nonlinear ICP devices. The nonlinear regime of the ICP quickly removes cations through a cation exchange membrane, which causes the displacement of anions moving towards the anode. As a result, the flat depletion zone propagates quickly, which is reminiscent of shock propagation[22]. Mani *et al.* called this dynamic the deionization (or depletion) shock[23]. To preconcentrate targets at a designated sensing position, preventing the expansion of the ion depletion zone is necessary, for example, by applying EOF or pressure-driven flow against the zone expansion[24]. Zangle *et al.*[22] clarified the criteria for ICP propagation in a one-dimensional model, and it highly depends on electrophoretic mobility[17], ionic strength[18], pH[25], and so on. This indicates that proper operating conditions will be altered according to the sample conditions.

Here, we present detailed design and experimental protocols for a novel ICP platform that preconcentrates targets within a spatiotemporally defined position[26]. The expansion of the ion depletion zone is blocked by the ion enrichment zone, leaving a stationary preconcentration plug at an assigned position, regardless of the operating time, applied voltage, ionic strength, and pH. This detailed video protocol is intended to show

the simplest method to integrate cation exchange membranes into microfluidic devices and to demonstrate the preconcentration performance of the new ICP platform compared to the conventional one.

Protocol

1. Fabrication of Cation Exchange Membrane-integrated Microfluidic Chips

1. **Preparation of silicon masters**
   1. Design two kinds of silicon masters: one for patterning a cation exchange resin and the other for building a microchannel with polydimethylsiloxane (PDMS).
      NOTE: The detail geometry will be described in the steps 1.3.1 and 1.4.1.
   2. Fabricate the silicon masters by using either conventional photolithography or deep reactive ion etching[27].
   3. Silanize the micropatterned silicon masters with trichlorosilane (~30 µL) in a vacuum jar for 30 min.
      CAUTION: Trichlorosilane is a pyrophoric liquid that is flammable and has an acute toxicity (inhalation, oral ingestion).

2. **Preparation of PDMS molds**
   1. Mix a silicone elastomer base with a curing agent at a 10:1 ratio and place the cup with this uncured PDMS (30-40 mL for replicating microstructures on a 4-in silicon wafer) in a vacuum jar for 30 min to remove the bubbles.
      NOTE: The silicone base contains siloxane oligomers terminating with vinyl groups and a platinum-based catalyst. The curing agent contains crosslinking oligomers that have three silicon-hydride bonds[28].
   2. Pour the uncured PDMS on the silicon masters, remove the bubbles with a blower, and cure the PDMS at 80 °C for 2 h in a convection oven.
   3. Detach the cured PDMS from the silicon masters and properly shape the PDMS with a knife (squared shapes, as shown in **Figure 2a-b, iv**).

3. **Patterning the cation exchange membranes**
   1. Cut half of the PDMS mold perpendicularly to the two parallel microchannels and punch holes at the ends of the PDMS channels with a 2.0-mm biopsy punch.
      NOTE: The PDMS mold for patterning the cation selective membrane has two parallel microchannels (width: 100 µm; height: 50 µm; interchannel distance: 100 µm; **Figure 1a**). The original shape of the mold can be imagined by mirroring the sliced mold along the cutting line. L-shaped microchannels are recommended for punching the two holes without overlapping.
   2. Clean a glass slide and the PDMS mold with tape and a blower and put the mold onto the glass slide to create reversible attachment between them.
   3. According to the microflow patterning technique[29], release ~10 µL of a cation exchange resin at the open end of the channel that was sliced in step 1.3.1 (**Figure 1b**). Place the syringe head on the punched holes and pull the plunger (black arrows in **Figure 1b**); a gentle negative pressure will pull the cation exchange resin, and the resin will fill the two channels.
      NOTE: It is recommended that the height of the microchannel is greater than 15 µm, because the high viscosity of the resin requires high pressure to fill the channels. On the other hand, it is better that the height does not exceed 100 µm, because the patterned ion selective membrane will become thicker than 1 µm; such a thick membrane may create a gap between the membrane and the PDMS channel[13].
   4. Detach the PDMS mold without touching the patterned resin and place the glass slide on the heater at 95 °C for 5 min to evaporate the solvent in the resin.
      NOTE: The thickness of the patterned membrane is usually less than < 1 µm. The mold is gently detached by hinging the mold to the open-ended side (dotted line and arrow in **Figure 1b**). It is best to detach the mold less than 1 min after filling the resin. If the mold is detached a few minutes later, thicker membranes could be obtained, but they would have a concave shape due to the capillary effect.
   5. Peel off the unnecessary part of the patterned membrane with a razor blade, making two separated line-patterns (**Figure 1c**).
      NOTE: The cation exchange material used here has perfluorinated groups, meaning the pattern is not strongly bonded to the glass. Therefore, the simple blading method can easily remove the unnecessary part of the membrane.

4. **Integration of the microchannel and the membrane-patterned substrate**
   1. Punch two holes at the ends of microchannels and another two holes where the membrane patterns will be located after bonding the PDMS channel to the membrane-patterned substrate fabricated in step 1.3.
      Note: The PDMS microchannel has one channel (width: 50-100 µm; height: 10 µm), but it is bonded to the ends of the neighboring channel (**Figure 1d**).
   2. Bond the PDMS microchannel to the membrane-patterned substrate immediately after oxygen plasma treatment for 40 s at 100 W and 50 mTorr.
      NOTE: Place the patterned membrane perpendicularly on the middle of the microchannel.

2. ICP Preconcentration

1. **Preparation for the experiment**
   1. Prepare various test solutions, including 1-100 mM KCl, 1 mM NaCl (pH ~7), the mixture of 1 mM NaCl and 0.2 mM HCl (pH ~3.7), the mixture of 1 mM NaCl and 0.2 mM NaOH (pH ~10.3), and 1x phosphate-buffered saline.
   2. Add a negatively charged fluorescent dye (~1.55 µM) to the test solutions.
      NOTE: The concentration of the added dye should be much lower than that of the salt ions (< 10 µM) so that the charged dyes do not contribute to an electrical current[30,31].

3. Load the sample solution in one reservoir of the channel and apply negative pressure to the other reservoir to fill the channel with the solution. Connect the two reservoirs hydrodynamically by releasing a large droplet to eliminate the pressure gradient along the channel (**Figure 2a**).
4. Fill the two reservoirs, which are connected to the cation exchange patterns, with buffer solutions (1 M KCl or 1 M NaCl) using a syringe or a pipet to compensate for the ICP effect in the reservoirs.
5. Place the wires at the reservoirs, across the two patterned membranes (anode on the left reservoir and cathode on the right), and connect them with a source measurement unit (**Figure 2a**).

2. **Visualization of the ICP phenomenon and ICP preconcentration**
   1. Load the ICP device on an inverted epifluorescence microscope. Apply a voltage (0.5100 V) and measure the current response with a source measurement unit.
   2. Capture fluorescent images with a charge-coupled device camera and analyze the fluorescent intensity using imaging software[32].

Representative Results

The schematic fabrication steps of a membrane-integrated microfluidic preconcentrator are shown in **Figure 1**. A detailed description of the fabrication is given in the Protocol. The designs and device images of the spatiotemporally defined preconcentrator[26] are contrasted with those of a conventional preconcentrator[11] (**Figure 2**). The ICP phenomenon in the spatiotemporally defined preconcentrator was investigated in terms of current-voltage-time responses and fluorescent intensity profiles (**Figure 3-4**). Similar to the ICP phenomenon with a single-membrane preconcentrator[3,11], three different regimes (Ohmic, limiting, and overlimiting) were observed in the current-voltage curve: 0.5-1 V (Ohmic and limiting) and 5 V (overlimiting). However, a nonconventional current recovery was detected in the current-time curve as the ion enrichment and the ion depletion zones merged. Next, the ICP preconcentration was tested at different times and voltages with the spatiotemporally defined preconcentrator (**Figure 5**) and the conventional one-membrane device (**Figure 6**). The preconcentration dynamics were quantified by fluorescence images, current-time responses, and fluorescent intensity graphs over different distances and times. When comparing the two platforms, the new ICP platform shows an advantage in always collecting targets (fluorescent dyes) between the two cation selective membrane patterns. In addition, it was confirmed that the preconcentration plug remains the same in different ionic strengths (1-100 mM NaCl) and pH values (3.7-10.3), verifying the high availability of the merging ICP preconcentrator in wide ranges of operating conditions (**Figure 7**). In **Figure 8**, a 10,000-fold protein preconcentration was also demonstrated.

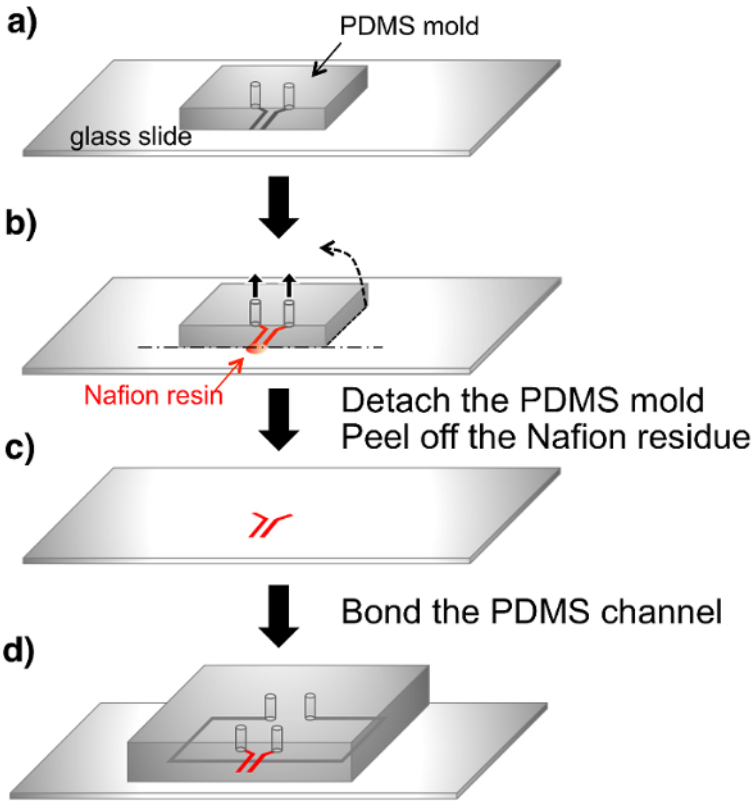

Figure 1. Fabrication steps of a cation exchange membrane-integrated microfluidic chip. After a PDMS mold is filled with a cation exchange resin using the microflow patterning technique (**a**-**c**)[29], the membrane-patterned glass substrate is bonded with a PDMS microchannel by oxygen plasma treatment (**d**). Please click here to view a larger version of this figure.

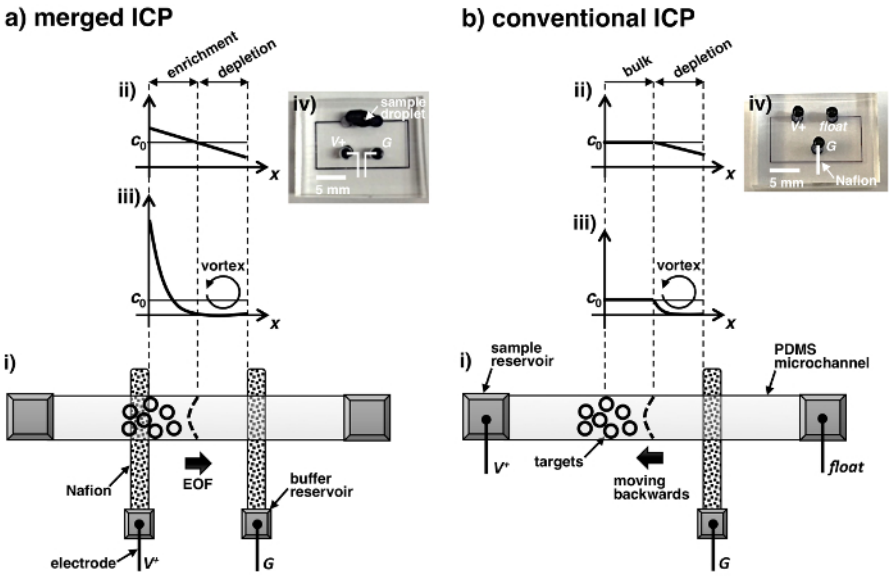

Figure 2. Schematics of the spatiotemporally defined preconcentrator (a) and conventional preconcentrator (b). (**a**) In the new platform, between two membrane patterns (i), ion depletion/enrichment zones are developed and merged together with linear (Ohmic and limiting regime; ii) or nonlinear (overlimiting regime; iii) concentration profiles. In all three current regimes, the ion enrichment zone blocks the propagation of the depletion zone and targets (hollow circles; i) are preconcentrated at the interface of the ion depletion and enrichment zones (curved, dotted line; i). The wall of the PDMS channel is negatively charged, and this generates electro-osmotic flow (EOF) between the two cation exchange membranes under an electric field. The EOF continuously delivers targets towards the interface of the depletion and enrichment zones. (**b**) In the conventional platform, only the ion depletion zone is developed near the membrane with linear (Ohmic and limiting regime; ii) and nonlinear (overlimiting regime; iii) concentration gradients. As the EOF delivers the targets, the preconcentration also occurs at the depletion zone boundary, but this zone (and the preconcentrated plug) moves away from the cation exchange membrane (black arrow; i). It is noted that there is no increase in the ion concentration here without the ion enrichment zone (ii-iii). In (a-b), the device images are shown in (iv). C_0 represents the initial ion concentration. V^+ and *G* indicate the anode and the cathode, respectively. Reprinted from Reference 26t with permission from The American Chemical Society. Please click here to view a larger version of this figure.

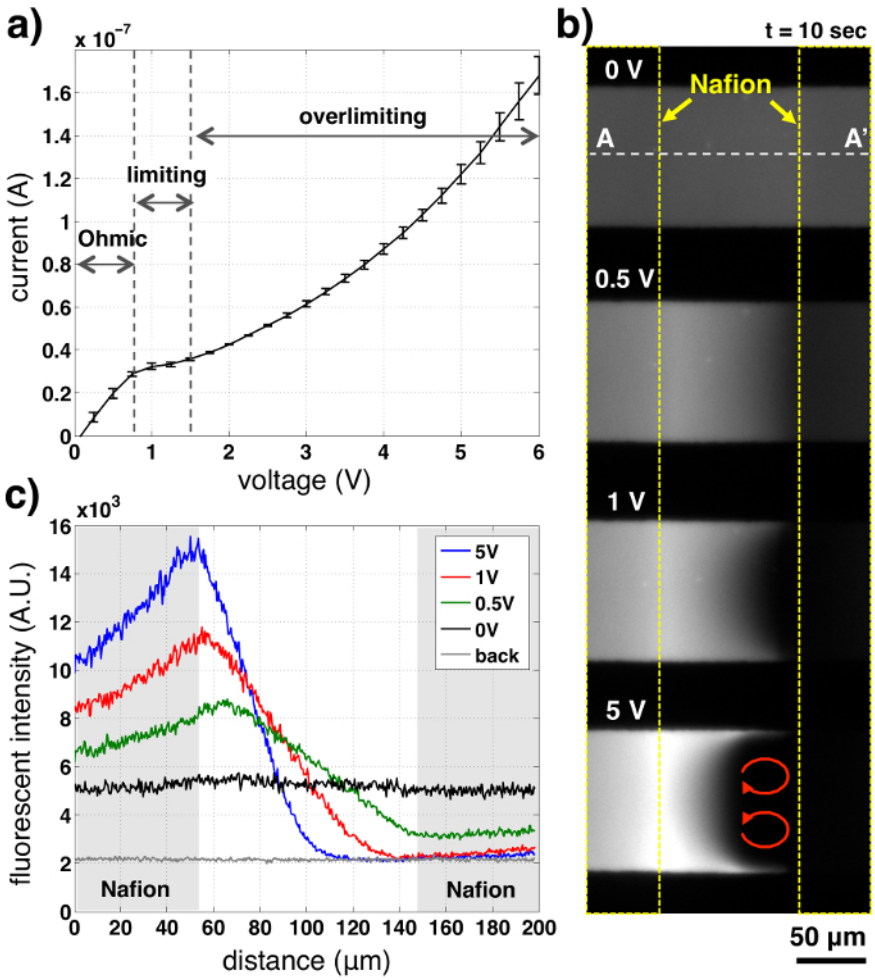

Figure 3. Merged ICP phenomenon between two cation exchange membranes. (**a**) The current-voltage curve shows three distinct regimes (Ohmic, limiting, and overlimiting). The current response is measured by ramping up the voltage at discrete intervals of 0.25 V every 40 s, which is repeated three times. The error bar indicates the standard deviation of the current responses. (b, c) In the three regimes, fluorescence images (**b**) and intensity profiles along A-A′ at the middle of the channel (**c**) were obtained. Yellow, dotted boxes indicate the locations of the cation selective membranes. 1 mM KCl solution with a 1.55 μM (1 μg/mL) negatively charged fluorescent dye was used. Reprinted from Reference 26 with permission from The American Chemical Society. Please click here to view a larger version of this figure.

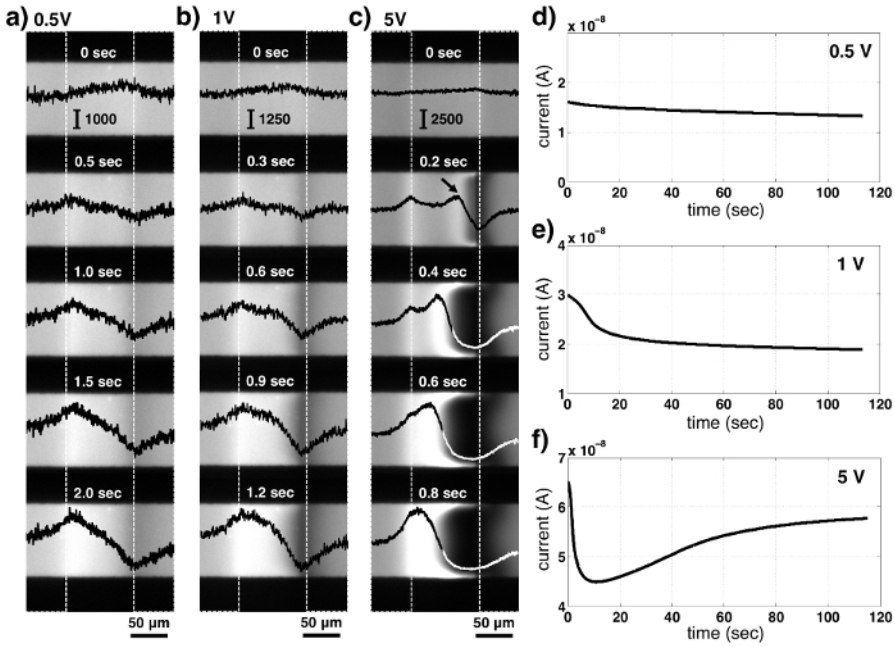

Figure 4. Transient dynamics of merging ion depletion and enrichment zones. (**a**, **b**) In the Ohmic-limiting regimes, the linear concentration gradients grow (< 1 s) from the cation exchange membrane and then overlap together (> 1 s). (**c**) In the overlimiting regime, the two ICP zones are merged more quickly (< 0.6 s) with the depletion shock (black arrow at 0.2 s). (**d**-**f**) The current-time responses show that the current is initially dropped due to the growth of the low-concentration depletion zone, which corresponds to low electrical conductivity. The current drop is then recovered due to a convective transport by vortices confined between two membranes. Reprinted from Referenced 26 with permission from The American Chemical Society. Please click here to view a larger version of this figure.

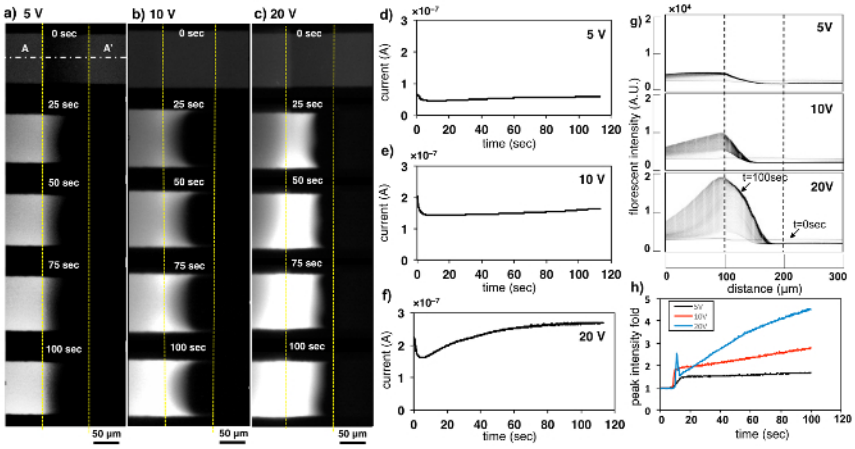

Figure 5. Spatiotemporally fixed preconcentration at 5, 10, and 20 V. (**a**-**c**) Fluorescence images of the merged ICP and the current-time responses (**d**-**f**) over time (0-100 s). The yellow, dotted lines indicate the location of the cation exchange membranes. (**g**) Time-lapse fluorescent intensity profiles are plotted along the microchannel (A-A′). The peak intensities increase as time passes, with fixed locations. (**h**) The peak intensity fold (*i.e.,* how many times greater than the initial fluorescent intensity). At higher voltages, the faster EOF delivers targets towards the interface of the ion depletion and enrichment zones, so the preconcentration speed increases. A spike at 20 V is induced by the depletion shock (**Figure 4c**). The fluorescent dyes accumulate on the shock boundary as it pushes the dyes. This initial accumulation is then somewhat dispersed when the depletion shock meets the ion enrichment zone, creating the spike in the peak intensity curve. As can be seen in **Figure 4c**, at 0.8 s, the peak was wider than it was at 0.4 s. This is probably because the left side of the left Nafion pattern (**Figure 2a**) was electrically floated, and the accumulated dyes could spread out. Reprinted from Reference 26 with permission from The American Chemical Society. Please click here to view a larger version of this figure.

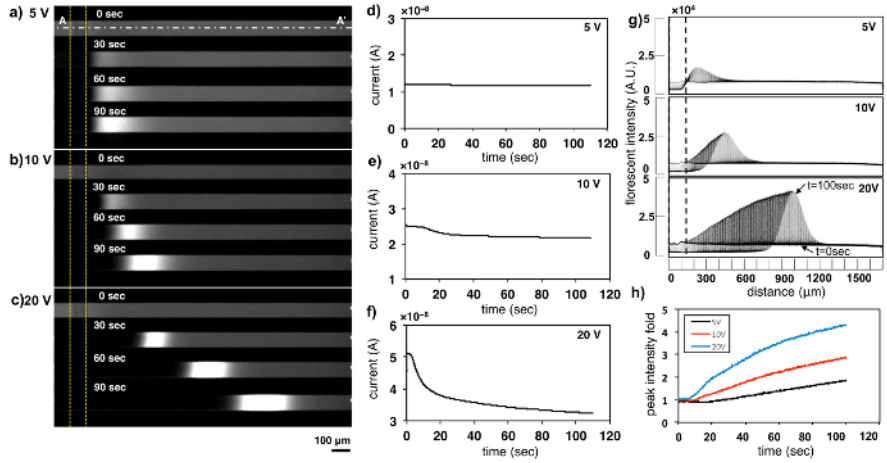

Figure 6. ICP phenomenon in the conventional ICP preconcentrator at 5, 10, and 20 V. (**a**-**c**) Fluorescence images of the ion depletion zone and the current-time response (**d**-**f**) over time (0-100 s). The propagation of the depletion zone and the preconcentration plug is clearly visualized in the fluorescence images. Accordingly, the vortices are not confined, so the current recovery does not occur, even in the overlimiting regime. Yellow, dotted lines mark the location of the cation exchange membranes. (**g**) Time-lapse fluorescent intensity profiles are plotted along the microchannel (A-A′). The peak intensities increase as time passes, but the location moves away from the membrane. (**h**) Peak intensity fold of the conventional ICP device. In contrast to the merged ICP device (**Figure 5h**), there is no intensity spike without the confinement of ICP zones, because the fluorescent intensity increased as the dye was preconcentrated. The increase of the peak intensity fold is similar to that of the merged ICP device at the same time (at a given voltage). This indicates that the length of time that the preconcentrated plug is held in place is crucial to the preconcentration performance. Please click here to view a larger version of this figure.

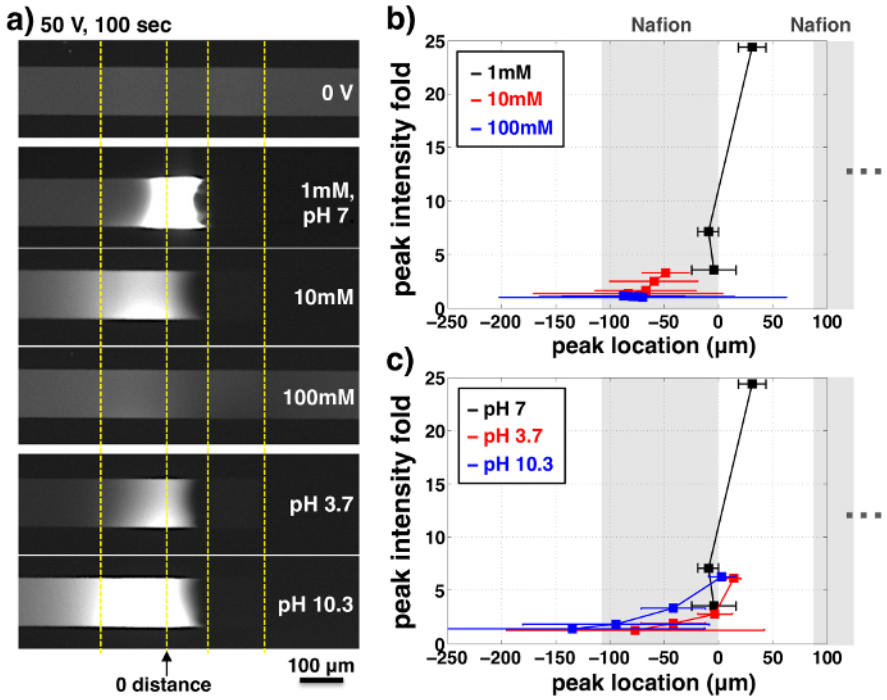

Figure 7. Spatiotemporally defined preconcentration at various ionic strengths (1-100 mM NaCl) and pH values (3.7-10.3). (**a**) Fluorescence images obtained after 100 s of operation at 50 V. As can be seen, the locations of the preconcentration plugs are still between the two cation exchange membranes (yellow, dotted lines), even though the intensity is weakened under high ionic strength and in a strong acidic or basic solution. (**b**, **c**) The location of the peak intensity and its intensity fold (*i.e.*, how many times greater than the initial intensity), mapped under 10, 20, 50, and 100 V. For a single condition (1, 10, 100 mM and/or pH 3.7, 7, and 10), there are four data points corresponding to the four voltage conditions. At higher voltages, there is a higher peak intensify fold in all cases. 100 V was not tested in 1 mM NaCl (pH 7) because the peak intensity already touched the highest values (due to the saturation of the camera) at 50 V. From the peak intensity profile, the peak region is also identified, with 1% below the peak intensity, which is represented by error bars (b, c). A higher voltage and a stronger EOF shift the peak location to the right, with a higher intensity fold and a sharper preconcentration plug. Gray boxes indicate the locations of the cation exchange membranes. The 0 distance (a) represents the origin of the x-axis (b, c), which is on the right edge of the left cation exchange membrane. The origin of the distance is the right edge of the left membrane. Reprinted from Reference 26 with permission from The American Chemical Society. Please click here to view a larger version of this figure.

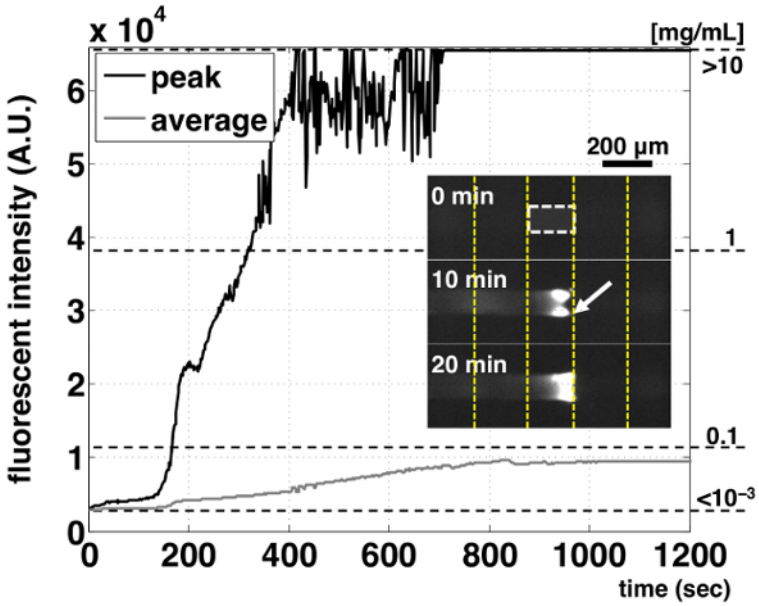

Figure 8. Demonstration of spatiotemporally fixed protein preconcentration. FITC-albumin (1 μg/mL) in 1x phosphate-buffered saline solution was used. 0.1% Tween 20 was also added to prevent nonspecific binding. Since the preconcentration is hardly achieved at a higher ionic strength (**Figure 7**), we doubled the width of the Nafion pattern (200 μm) and used a narrower PDMS channel (50 μm). In this way, the performance of ICP preconcentration was enhanced by broadening the ion pathway and reducing the absolute amount of ions in the channel. At an applied voltage of 100 V, the peak and averaged fluorescent intensities were traced in the white, dotted box, which is the region between the two cation exchange membranes. Within 10 min of operation, the proteins were preconcentrated up to 10 mg/mL (peak) and ~0.1 mg/mL (averaged), indicating 10,000- and 100-fold preconcentrations, respectively. The inset fluorescence images were obtained at 0, 10, and 20 min. In this work, a 20-min operation was enough to preconcentrate the target molecules, so we did not cover longer operating times. Reprinted from Reference 26 with permission from The American Chemical Society. Please click here to view a larger version of this figure.

Discussion

We have described the fabrication protocol and the performance of a spatiotemporally defined preconcentrator in a range of the applied voltage (0.5-100 V), ionic strength (1-100 mM), and pH (3.7-10.3), achieving a 10,000-fold preconcentration of dyes and protein within 10 min. As like previous ICP devices, the preconcentration performance becomes better at higher voltage and at lower ionic strength. One additional parameter we can consider here is the distance between two cation exchange membranes. If we increase the inter-membrane distance, the electric field decreases under the same applied voltage, resulting in the decrease of the preconcentration speed[26].

The microflow patterning technique[29] used in this work is a robust method for patterning cation exchange resins, so it has been one of the gold-standard methods for integrating the ion exchange materials into microfluidic systems. Nevertheless, it is necessary to fabricate two juxtaposed cation exchange membranes with a short intermembrane distance (smaller than few hundred micrometers). In steps 1.3.3-1.3.4, the cation exchange resin is in a liquid phase. Therefore, the resin in the two microchannels can be collapsed, and the remaining resin drop at the open end of the channels can also flood during the mold detachment (step 1.3.4.). To build two cation exchange membranes with high pattern fidelity, we used the resin with a relatively high viscosity (20% of the cation exchange material in the solvents) and carefully set the detachment process with a designated detaching direction.

Even though the high operating flexibility of this platform was demonstrated, the reader might be concerned about determining the optimal conditions from the wide range within the operating window. One representative trade-off is between the preconcentration speed and the stability of the ICP effect. As can be seen in Figure 5 in Kwak *et al.*[26], a high applied voltage (> 50 V) can condense targets quickly; however, this also induces strong vortices in the depletion zone (1 mM / pH 7 in **Figure 7a**), which decreases the stability of the sample preconcentration. Accordingly, the preconcentration speed becomes difficult to predict[33]. In the current stage, we recommend experimental conditions with a relatively low voltage (< 30 V) and ionic strength (< 10 mM) for a stable, predictable, and spatiotemporally fixed preconcentration. This trade-off between the preconcentration speed and the stability of the preconcentrated plug is also related to the sources of the nonlinear ICP (surface conduction, EOF, and electro-osmotic instability). The main source of the nonlinear ICP at a relatively small voltage (< 50 V) is EOF, creating a coherent vortex pair in the depletion zone (**Figure 3b**), which leads to a stable preconcentration. At a relatively high voltage (> 50 V), the main source of the nonlinear ICP is changed to electro-osmotic instability, resulting chaotic multiple vortexes, which decrease the stability of the preconcentration.

Recently, paper-based ICP platforms have been developed by Phan *et al.*[34], Gong *et al.*[19], and Han *et al.*[21]. These paper devices with microporous structures can suppress electro-osmotic instability[4,35] and alleviate the stability issue. However, the sizes of the paper channels are generally about 0.5-5 mm, which is much bigger than a conventional microfluidic channel. This wider paper channel with random fiber networks causes irregular motions in the preconcentrated plugs. This has been inevitable in paper-based ICP preconcentrators, because the minimum feature size of wax patterning and paper cutting (*i.e.,* fabrication methods to build paper channels) is about few hundred micrometers.

The ICP preconcentrator has been used in a wide range of biomicrofluidic platforms for preconcentrating various bio-agents; amplifying the signals of various assays; and detecting targets, such as therapeutic proteins[36], peptides[37], aptamers[17], and enzymes[38]. These previous works targeted fluorescence-labeled biomolecules. This is because we cannot specify the exact operating conditions (*i.e.,* voltage and flow rate) to maintain the preconcentration site, so we first need to find the proper conditions for the preconcentrator targets. Departing from previous work, the merged ICP phenomenon allows us to always fix the preconcentrated plugs at a broad range of operating conditions while maintaining the high flexibility of the ICP devices. For example, we can modulate the merged ICP system with a tangential fluid flow, and operate it in the continuous-flow mode[39]. This indicates that we can now extend the applications of ICP preconcentrators to label-free detection techniques without using visualization instruments and tracers. This unique advantage of the spatiotemporal controllability provides a strong commercial opportunity to integrate the ICP device with generic benchtop platforms, such as polymerase chain reaction machines and mass spectrometers.

Disclosures

The authors have nothing to disclose.

Acknowledgements

This work was supported by the internal fund of the Korea Institute of Science and Technology (2E26180) and by the Next Generation Biomedical Device Platform program, funded by the National Research Foundation of Korea (NRF-2015M3A9E202888).

References

1. Probstein, R. F. *Physicochemical Hydrodynamics: An Introduction*, *2nd ed.* Wiley-Interscience. New York (2003).
2. Strathmann, H. *Ion-Exchange Membrane Separation Processes.* Elsevier. Amsterdam (2004).
3. Dydek, E.V., *et al.* Overlimiting Current in a Microchannel. *Phys. Rev. Lett.* **107** (11), 118301 (2011).
4. Kwak, R., Pham, V.S., Lim, K.M., & Han, J. Shear flow of an electrically charged fluid by ion concentration polarization: scaling laws for electroconvective vortices. *Phys. Rev. Lett.* **110** (11), 114501 (2013).
5. Rubinstein, I., & Zaltzman, B. Electro-osmotically induced convection at a permselective membrane. *Phys. Rev. E.* **62** (2), 2238-2251 (2000).
6. Kwak, R., Kim, S., & Han, J. Continuous-flow biomolecule and cell concentrator by ion concentration polarization. *Anal. Chem.* **83** (19), 7348-7355 (2011).
7. Jeon, H., Lee, H., Kang, K.H., & Lim, G. Ion concentration polarization-based continuous separation device using electrical repulsion in the depletion region. *Sci.Rep.* **3**, 3483 (2013).
8. Kim, S.J., Ko, S.H., Kang K.H., & Han, J. Direct seawater desalination by ion concentration polarization. *Nat. Nanotechnol.* **5** (4), 297-301 (2010).
9. MacDonald, B.D., Gong, M.M., Zhang, P., & Sinton, D. Out-of-plane ion concentration polarizationfor scalable water desalination. *Lab Chip.* **14** (4), 681-685 (2014).
10. Schoch, R.B., Han, J., & Renaud, P. Transport phenomena in nanofluidics. *Rev.Mod. Phys.* **80** (3), 839-883 (2008).
11. Kim, S.J., Song, Y.A., & Han, J. Nanofluidic concentration devices for biomolecules utilizing ion concentration polarization: theory, fabrication, and applications. *Chem. Soc. Rev.* **39** (3), 912-922 (2010).
12. Mai, J.Y., Miller, H., & Hatch, A.V. Spatiotemporal mapping of concentration polarization Induced pH changes at nanoconstrictions. *ACS Nano.* **6** (11), 10206-10215 (2012).
13. Kim, B., *et al.* Tunable ionic transport for a triangular nanochannel in a polymeric nanofludic system. *ACS Nano.* **7** (1), 740-747 (2013).
14. Syed, A. Mangano, L. Mao, P.Han J., & Song, Y.-A. Creating sub-50 nm nanofluidic junctions in a PDMS microchip via self-assembly process of colloidal silica beads for electrokinetic concentration of biomolecules. *Lab Chip.* **14**, 4455-4460 (2014).
15. Wang Y.C., Stevens, A.L., & Han, J., Million-fold preconcentration of proteins and peptides by nanofluidic filter. *Anal. Chem.* **77** (14), 4293-4299 (2005).
16. Lee, J.H., Cosgrove, B.D., Lauffenburger, D.A., & Han, J. Microfludic concentration-enhanced cellular kinase activity assay. *J. Am. Chem. Soc.* **131** (30), 10340-10341 (2009).
17. Cheow, L.F., & Han, J. Continuous signal enhancement for sensitive aptamer affinity probe electrophoresis assay using electrokinetic concentration. *Anal. Chem.* **83** (18), 7086-7093 (2011).
18. Ko, S.H., *et al.* Nanofluidic preconcentration device in a straight microchannel using ion concentration polarization. *Lab Chip.* **12** (21), 4472-4482 (2012).
19. Gong, M.M., Nosrati, R., Gabriel, M.C.S., Zini, M., & Sinton, D. Direct DNA analysis with paper-based ion concentration polarization. *J. Am. Chem. Soc.* **137** (43), 13913-13919 (2015).
20. Hong, S., Kwak, R., & Kim, W. Paper-based flow fractionation system applicable to preconcentration and field-flow separation. *Anal. Chem.* **88** (3), 1682-1687 (2016).
21. Han, S.I., Hwang, K.S., Kwak, R., & Lee, J.H. Microfluidic paper-based biomolecule preconcentrator based on ion concentration polarization. *Lab Chip.* **16**, 2219-2227 (2016).
22. Zangle, T.A., Mani, A., & Santiago, J.G. Theory and experiments of concentration polarization and ion focusing at microchannel and nanochannel interfaces. *Chem. Soc. Rev.* **39** (3), 1014-1035 (2010).
23. Mani, A., & Bazant, M.Z. Deionization shocks in microstructures. *Phys. Rev. E.* **84**, 061504 (2011).
24. Slouka, Z., Senapati, S., & Chang, H.C. Microfluidic systems with ion-selective membranes. *Annu. Rev.Anal. Chem.* **7**, 317-335 (2014).
25. Kirby, B.J., & Hasselbrink, E.F. Zeta potential of microfluidic substrates: 1. Theory, experimental techniques, and effects on separations. *Electrophoresis.* **25** (2), 187-202 (2004).
26. Kwak, R., Kang, J.Y., & Kim, T.S. Spatiotemporally defining biomolecule preconcentration by merging ion concentration polarization. *Anal. Chem.* **88** (1), 988−996 (2016).
27. Duffy, D.C., McDonald, J.C., Schueller, O.J.A., & Whitesides, G.M. Rapid prototyping of microfluidic systems in poly(dimethylsiloxane). *Anal. Chem.* **70** (23), 4974-4984 (1998).

28. Campbell, D.J., *et al.* Replication and compression of surface structures with polydimethylsiloxane elastomer. *J. Chem. Educ.* **76**(4), 537-541 (1999).
29. Lee, J.H., Song, Y.A., & Han, J. Multiplexed proteomic sample preconcentration device using surface-patterned ion-selective membrane. *Lab Chip.* **8** (4), 596-601 (2008).
30. Kwak, R., Guan, G., Peng, W.K., & Han, J. Microscale electrodialysis: concentration profiling and vortex visualization. *Desalination.* **308**, 138-146 (2013).
31. Chambers, R.D., & Santiago, J.G. Imaging and quantification of isotachophoresis zones using nonfocusing fluorescent tracers. *Anal. Chem.* **81**, 3022-3028 (2009).
32. Rasband, W.S., *ImageJ.* U. S. National Institutes of Health, Bethesda, Maryland, USA, http://imagej.nih.gov/ij/, 1997-2016 (2016).
33. Minerick, A.R., Ostafin, A.E., & Chang, H.C. Electrokinetic transport of red blood cells in microcapillaries. *Electrophoresis.* **23** (14), 2165-2173 (2002).
34. Phan, D-.T., Shaegh, S.A.M, Yang, C., & Nguyen, N-.T. Sample concentration in a microfluidic paper-based analytical device using ion concentration polarization. *Sens. Actuators B.* **222**, 735-740 (2016).
35. Rubinstein, S.M., Direct observation of a nonequilibrium electro-osmotic instability. *Phys. Rev. Lett.* **101**, 236101 (2008).
36. Ouyang, W., *et al.* Microfluidic platform for assessment of therapeutic proteins using molecular charge modulation enhanced electrokinetic concentration assays. *Anal. Chem.* **88**, 9669-9677 (2016).
37. Cheow, L.F., Sarkar, A., Kolitz, S., Lauffenburger, D., & Han, J. Detecting kinase activities from single cell lysate using concentration-enhanced mobility shift assay. *Anal. Chem.* **86**, 7455-7462 (2014).
38. Chen, C.-H., *et al.* Enhancing protease activity assay in droplet-based microfluidics using a biomolecule concentrator. *J. Am. Chem. Soc.* **133**, 10368-10371 (2011).
39. Kwak, R., Pham, V.S., Kim, B., Lan C., & Han, J. Enhanced salt removal by unipolar ion conduction in ion concentration polarization desalination. *Sci. Rep.* **6**, 25349 (2016).

